Heliyon 10 (2024) e40923

Contents lists available at ScienceDirect

Heliyon

journal homepage: www.cell.com/heliyon

Review article

Optical sensors based on plasmonic nano-structures: A review

Shiva Khani *, Pejman Rezaei

Faculty of Electrical and Computer Engineering, Semnan University, Semnan, Iran

ARTICLE INFO

Keywords:
Optical
Sensitive sensor
Tunable sensor
Metal-insulator-metal waveguide
Surface plamon polaritons
plasmonic sensor

ABSTRACT

Optical sensors are among the most significant optical devices that have found extensive applications for THz sensing. Surface plasmon-based sensors have attracted increasing attention more than other kinds of optical sensors such as photonic crystal, optical fiber, and graphene sensors, owing to their compact footprint, fast reaction, and high sensitivity value. Therefore, this work reviews plasmonic sensor structures divided into three general categories. These category types are plasmonic sensors based on conventional basic platforms, coupled resonator structures, and periodic structures. Furthermore, periodic structures include two sub-categories named metal-insulator and insulator-insulator periodic structures. The most prevalent methods used to investigate such sensors are the finite element method (FEM) and finite-difference time-domain (FDTD) method. Also, the metal and insulator materials used are usually silver, gold, air, Si, SiO_2, and so on. Based on the noted features, such sensors have obtained specific attention for many applications in chemistry, physics, and biomedical.

1. Introduction

Due to the requirements of ultra-high computational speeds, semiconductor devices [1–3] cannot realize all future developing requirements. Therefore, achieving devices with less noise and higher information densities made researchers switch from electronic circuits [4–6] to photonic circuits [7–10]. One of the appropriate candidates to replace electronic integrated circuits is photonic crystal (PC) structures [11–13]. PCs [14,15] are periodic topologies that can control the light flow. PCs can be designed and fabricated into three groups of 1D, 2D, and 3D structures. The periodicity of PC structures generates photonic band gaps (PBGs) with sharp edges that cause them to perform as an ideal mirror and confine light in the waveguide (WG) [16]. Accordingly, they can be applied to design high-sensitivity optical sensors [17–19] and high contrast ratio optical switches [20,21].

Mentioned merits also make PCs an attractive structure for designing other optical topologies. Such devices include PC resonators [22], sensors [23], filters [24–26], demultiplexers [27–29], splitters [30,31], couplers [32,33], modulators [34,35], logic gates [36–38], oscillators [39], and so on. Although a variety of high-performance optical devices can be designed and fabricated using PC structures, the relatively large footprints of such structures can be considered as a disadvantage. Accordingly, most optical devices designed based on PCs can be realized using other optical structures such as surface plasmon-based structures [40–42] with fewer footprint areas.

Surface plasmon polaritons (SPPs) are surface electromagnetic waves excited at the metal-insulator (MI) interfaces [43]. In other words, plasmons are hybrid electron-photon oscillation that occur at the interface between a conductor and a dielectric [44]. As mentioned, plasmonic structures [45] are one of the best options for realizing nanoscale devices. This is because of the capability of

* Corresponding author.
E-mail address: shiva.khani@semnan.ac.ir (S. Khani).

https://doi.org/10.1016/j.heliyon.2024.e40923
Received 30 September 2024; Received in revised form 29 November 2024; Accepted 3 December 2024
Available online 4 December 2024

SPP waves to break the prevalent diffraction limit of light in usual photonic devices [46,47]. Recently, numerous SPP-based nanostructures have been designed and experimentally or theoretically studied such as plasmonic sensors [48–50], filters [51–54], splitters [55,56], demultiplexers [57,58], absorbers [59], converters [60], switches [61–63], logic gates [64,65], modulators [66,67], and so on.

Among optical devices, sensors [68] have been the center of attention due to their wide applications. Their applications are in different areas such as chemistry [69], physics [70], biomedical [71], and so on. For example, they can be used for blood component measurements [72], health care applications [73], cancer cell detections [74], temperature sensing applications [75], and so on. Based on Fig. 1 (various frequency bands in the electromagnetic (EM) spectrum and their nomenclature according to the IEEE Std [76]), besides optical sensors, there are other kinds of sensors such as radio frequency (RF) [77,78], microwave [79–81], Millimeter Wave (mmW) [82,83], and THz [84,85] sensors for different frequency ranges. In an overall comparison between optical sensors and other types, it can be said that capacitive sensing using microstrip structures, interdigitated capacitors, and resonators is employed for RF, microwave, mmW, and THz sensors. In contrast, optical sensors use common methods such as quantum dots, PCs, surface plasmon resonance, ellipsometry, surface-enhanced Raman scattering, fluorescence, laser Doppler flowmetry, and backscattering [86]. On the other hand, as known, when the frequency is increased, several factors come into play that lead to a decrease in the size of the devices, and this trend is driven by higher performance for devices [87,88]. Accordingly, optical sensors have a more compact size and better performance compared to the other types of sensors [89–91]. Until now, different methods have been approved to realize optical sensors. These approaches are based on different structures such as optical fiber topologies [92,93], graphene [94,95], PC [96,97], plasmonic [98,99], and so on.

Due to the sensitivity of surface plasmons to changing the refractive index (RI) of its insulator material, this structure may be applied as a gadget for optical sensing. In plasmonic sensors, RI changes can be detected by connecting the particle to the surface. It means that the particle-to-surface connection does not require labeling and is converted straight into a signal, while conventional optical sensors require chromophore colors. Plasmon-based sensors increase main factors such as sensitivity, tunability, optical usability, and stability of such sensors in the living ambiance compared to usual optical sensors. Consequently, surface plasmon sensors can overcome the restrictions of other common optical sensors. The prevalent topologies to design optical surface plasmon-based sensors are plasmonic ring-shaped resonators [100,101], Mach-Zehnder interferometers [102], cross-shaped resonators [103], nanodisk resonators [104], rectangular resonators [105,106], triangular resonators [107], and so on.

This paper discusses a centralized review of optical surface plasmon-based sensors. In this paper, different topologies that are used to design plasmonic sensors are divided into three general categories named plasmonic sensors based on conventional basic platforms, coupled-resonator structures, and periodic structures. Using periodic structures is divided into two types; MI and insulator-insulator (II) periodic structures. This paper is arranged in this way. Following the introduction section, conventional principal platforms that are used to design plasmonic sensor structures and evaluation parameters for sensing performance are introduced in section 2. Section 3 explains different techniques for designing plasmonic sensor structures. Section 4 discusses the fabrication technology of different types of plasmonic sensors. The sensing performance of designed sensors is compared in section 5, and the future of plasmonic sensors is discussed in section 6. Finally, the last section is dedicated to conclusions.

2. Conventional basic platforms for plasmonic sensors and evaluation parameters for sensing

Optical plasmonic sensors benefit from significant features such as small footprints, simplicity in the fabrication process, and remote sensing applications [108,109]. Consequently, they have attracted a lot of consideration, recently. In addition, such sensors can act better than other traditional optical sensors in terms of some factors such as sensitivity, tuneability, ultra compactness, and effective light confinement [110]. To simulate plasmonic sensors and achieve high sensitivity, noble metals such as gold and silver are commonly used [111]. Also, when nanostructured materials such as Molybdenum disulfide, black phosphorous, and graphene are combined with noble metals, a higher sensitivity value is achieved [112]. Accordingly, plasmonic sensors are suitable options for different applications such as biomedical, chemistry, and physics [113–115].

Plasmonic optical sensor structures can be classified into different types of basic platforms. Fig. 2 shows the most conventional platforms used for designing plasmonic sensors. Such platforms consist of a resonator and metal-insulator-metal (MIM) WGs. Fig. 2(a) shows a resonator coupled to two WGs. Such a structure works as a band-pass filter. Fig. 2(b) shows a resonator laterally coupled to a WG. Such a structure generates a narrow-band band-stop filter. A ring resonator-based structure that also acts as a band-pass filter is

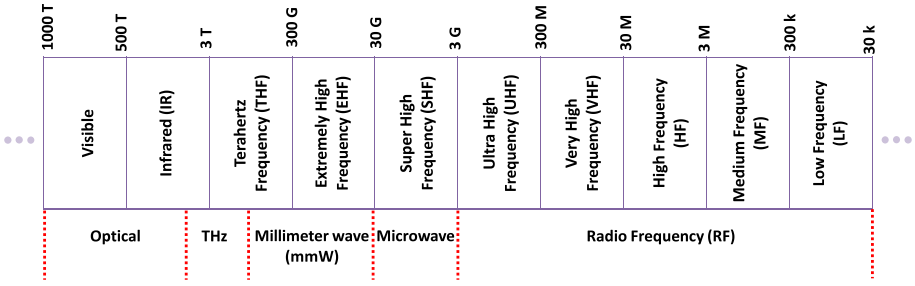

Fig. 1. EM spectrum showing different band ranges [76].

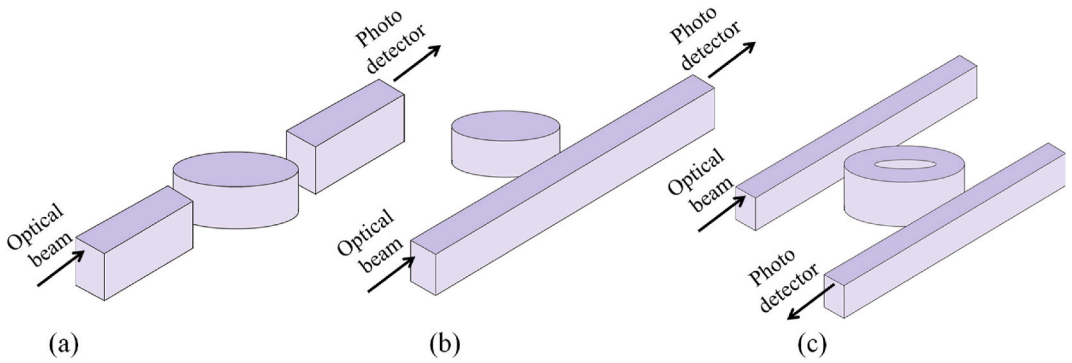

Fig. 2. Conventional basic platforms used for designing plasmonic sensors, (a) A resonator coupled to two WGs from both sides, (b) A resonator coupled to a WG from one side, (c) Ring resonator-based platform.

demonstrated in Fig. 2(c).

In these topologies, the insulator regions are usually exposed to the analyte. By varying the RI of the analyte, the transmission spectrum changes. To give a better perspective of the performance of the sensor, it is assumed that the transmittance of a hypothetical narrow-band band-pass structure is a single-mode Lorentzian spectrum (black solid curve in Fig. 3). As seen, when the RI of the analyte is varied from n_0 to $n_0+\Delta n$, the Lorentzian resonance frequency (ω_{res}) shifts to a lower frequency ($\omega_{res}-\Delta\omega$). Two main parameters are defined to be able to compare the performance of different plasmonic sensors. The first one is the sensitivity of plasmonic sensors (S_λ). The resonance wavelength shift ($\Delta\lambda$) for a given RI change (δn) is compared by this parameter that is provided by Eq. (1) [116,117]:

$$S_\lambda(\lambda)=\frac{\partial\lambda_{res}}{\partial n_{analyte}}\simeq\frac{\Delta\lambda}{\delta n}\quad\left(\frac{nm}{RIU}\right) \tag{1}$$

Although the sensitivity parameter is discussed in most published works, it cannot be a comprehensive parameter for comparison. This parameter cannot show the resolution between the two primary and shifted resonance wavelengths. Accordingly, two sensors with the same sensitivity may have different resolutions. Therefore, a more comprehensive parameter named the figure of merit (FoM) is specified for comparing the performance of plasmonic sensors. The FoM parameter is given by Eq. (2) [116,117]:

$$\mathrm{FoM}=\frac{S_\lambda(\lambda)}{\Gamma}\quad\left(RIU^{-1}\right) \tag{2}$$

The FoM parameter is the ratio of S_λ to the bandwidth of the resonance mode (Γ). The bandwidth is the wavelength range that light can pass through the structure with minimal attenuation. The wavelength at which the transmittance level of the signal decreases by 3 dB from its maximum value is called the 3 dB bandwidth. A 3 dB decrease in transmittance means the signal value becomes half of its maximum value. The bandwidth of an ideal band-pass structure (a structure with 100 % transmittance value at its resonance mode) is specified in Fig. 3.

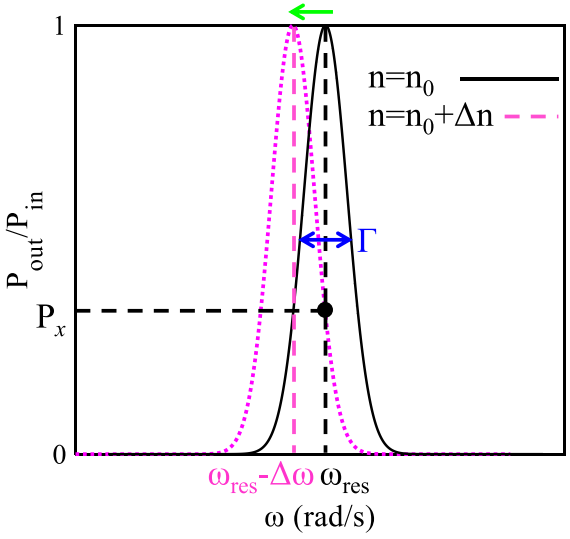

Fig. 3. Lorentzian resonance of a hypothetical narrow-band band-pass structure and its shifted resonance.

Accordingly, a sensor with a high value for FoM parameter results in a high-performance sensor. Next, it will be studied how a high value for the FoM parameter of this case investigated here can be achieved. Perturbation theory can be used for this purpose [118].

According to the perturbation theory, if the analyte of a sensor is exposed to a slight variation, the corresponding resonance shift can be estimated by Ref. [118]:

$$\frac{\Delta\omega}{\omega_{res}} = -\frac{\iiint_V \left(\delta_\mu |H_{res}|^2 + \delta_\varepsilon |E_{res}|^2\right).dV}{\iiint_V \left(\mu |H_{res}|^2 + \varepsilon |E_{res}|^2\right).dV} = -\frac{1}{W}\iiint_V \left(\frac{\delta_\varepsilon}{\varepsilon}.W_e + \frac{\delta_\mu}{\mu}.W_m\right).dV \tag{3}$$

Where H_{res}, W_m, and μ are the original magnetic field, magnetic energy density, and original permeability, respectively. In addition, E_{res}, W_e, and ε are the original electric field, electric energy density, and original permittivity, and W is the total energy stored in the analyte. When μ does not change, Eq. (3) can be rewritten as Eq. (4):

$$\frac{\Delta\omega}{\omega_{res}} = -\frac{1}{W}\iiint_V \left(\frac{\delta_\varepsilon}{\varepsilon}.W_e\right).dV = -\frac{1}{W}\iiint_V \left(\delta\varepsilon_r\varepsilon_0 |E_{res}|^2\right).dV \tag{4}$$

Here ε_0 is the permittivity of the free space, and ε_r is the relative permittivity. Moreover, the RI (n) can be shown by Eq. (5).

$$n = \sqrt{\varepsilon_r.\mu_r} \tag{5}$$

Here μ_r shows the relative permeability. Consequently, the optical shift ($\Delta\omega$) can be obtained by Eq. (6) [119]:

$$\frac{\Delta\omega}{\omega_{res}} = -\sigma\frac{\delta n}{n} \tag{6}$$

Where δn is the RI change, and σ is related to the portion of resonance mode energy kept in the analyte. This formula shows that by increasing the resonance mode energy, the frequency shift increased. Furthermore, a Lorentzian function is shown by Eq. (7). In this equation, P_{in} is the input power, and P_{out} shows the transmitted power.

$$\frac{P_{out}}{P_{in}} = \frac{1}{1 + \left(\frac{2(\omega-\omega_{res})}{\Gamma}\right)^2} \tag{7}$$

The quality factor (Q-factor) is defined by Eq. (8) [120,121]:

$$Q = \frac{\omega_{res}}{\Gamma} \tag{8}$$

Fig. 3 shows that the power ratio of the resonance frequency (ω_{res}) for the primary and perturbed cases are considered to be unity and P_x, respectively. The value of P_x can be given by:

$$P_x = \frac{1}{1 + \left(\frac{2\Delta\omega}{\Gamma}\right)^2} = \frac{1}{1 + \left(2Q\frac{\Delta\omega}{\omega_{res}}\right)^2} = \frac{1}{1 + \left(2Q\sigma\frac{\delta n}{n}\right)^2} \tag{9}$$

As a result, the contrast ratio (CR) is given by Eq. (10). In this equation, the power ratio of the unperturbed resonator is equal to 1, and the power ratio of the perturbed resonator is shown by P_x.

$$CR = \frac{1}{P_x} = 1 + \left(2Q\frac{\Delta\omega}{\omega_{res}}\right)^2 \simeq 4Q^2\left(\frac{\Delta\omega}{\omega_{res}}\right)^2 \tag{10}$$

To realize a high FoM plasmonic sensor, it is necessary to increase the CR value. Also, to earn a high value for the CR parameter, P_x must be as close to zero as possible. Eq. (9) shows that by enhancing the Q-factor and σ values, P_x reduces. Finally, the footprint of the plasmonic sensor is another effective evaluation parameter, so that a smaller size is more desirable. The ideal design structure for a surface plasmon-based topology as a sensor is one of the most attractive research areas. This study area has been considered for years. Accordingly, the various structures of the plasmonic sensors have been discussed in the following section.

3. Different techniques to design plasmonic sensor structures

Different techniques for realizing plasmonic sensors can be organized into three general types. The first one is that plasmonic sensors are created using conventional basic platforms. Such a technique has been utilized in most of the papers by using different types of resonator shapes. Another technique is that by coupling more than one resonator in the conventional basic platforms, plasmonic sensors can be designed. Using periodic structures is the third method which is separated into two categories, namely MI and II periodic topologies. Each of the above techniques is briefly considered in this section.

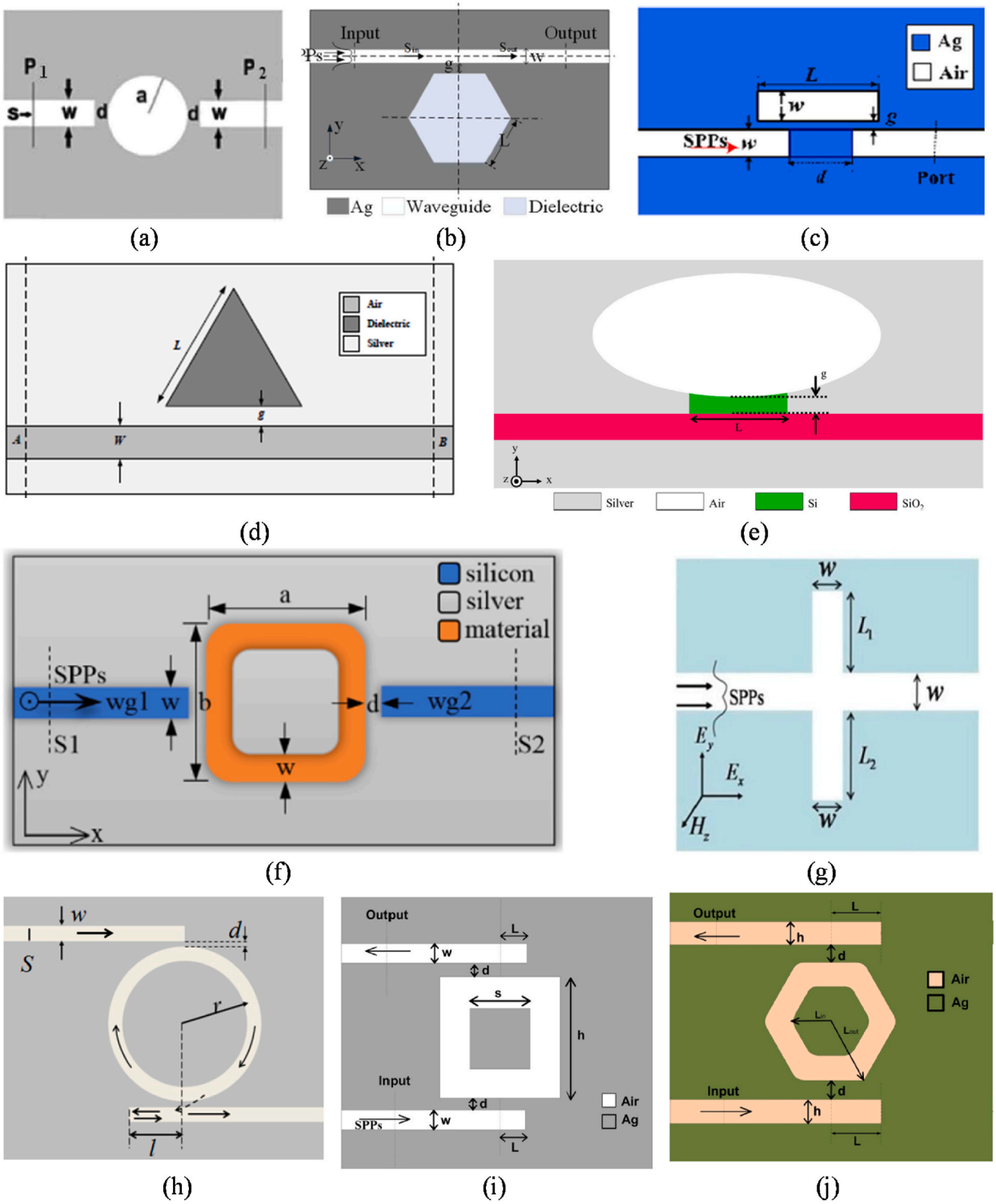

Fig. 4. Examples of plasmonic sensors based on basic platforms: (a) Disk resonator [122], (b) Hexagonal resonator [123], (c) Rectangular resonator [124], (d) Triangular resonator [125], (e) Elliptical resonator [126], (f) Rectangular ring-shaped resonator [127], (g) Stub resonators [128], Ring resonator-based structure using a (h) disk ring [129], (i) square ring [130], (j) hexagonal ring [131].

3.1. Plasmonic sensors based on conventional basic platforms

The most simple plasmonic sensor structures that have been used in various published works are based on a resonator coupled to MIM WGs (conventional basic platforms in Fig. 2). A variety of plasmonic sensors with different resonator types based on the basic platforms have been designed so far. Fig. 4 shows some of these plasmonic sensor structures. In Ref. [122], to design a plasmonic RI sensor (RIS), a disk resonator coupled to two MIM plasmonic WGs (Fig. 4(a)). Disk resonators have some advantages such as easy design and fabrication process and tunable resonance wavelengths. Accordingly, such a resonator is one of the most widely used structures in surface plasmon-based devices. The proposed structure generated two resonance wavelengths in the range of 500–1000 nm. The locations of these resonance wavelengths depend on the RI of the insulator material which is positioned into the disk resonator and MIM WGs. The finite-difference time-domain (FDTD) simulations showed that the sensitivity of the suggested sensor was 357.1 nm/RIU for the resonance mode of 1, and 222.2 nm/RIU for the resonance mode of 2. This sensor was used to identify various materials.

Another resonator type that has been used in Ref. [123] is the hexagonal resonator (Fig. 4(b)). The main advantage of hexagonal resonators is their better coupling capability with MIM WGs than disk resonators. In contrast, the fabrication procedure of hexagonal resonators is more difficult than disk resonators. In this structure, the hexagonal resonator was filled with the analyte. The structure performance was analyzed using the FDTD method, and its sensitivity and FoM were 1562.5 nm/RIU and 38.6 RIU^{-1}, respectively. Since the topology designed in this work can act for temperature sensing, its temperature sensitivity was also calculated using $S_T = \frac{\Delta\lambda}{\Delta T}\left(\frac{nm}{o_C}\right)$ and obtained 0.456 $\frac{nm}{o_C}$.

Using rectangular [124] and triangular [125] resonators with strong coupling capabilities are other methods for designing plasmonic sensors. In Ref. [124], by coupling a rectangular resonator to two MIM WGs, a plasmonic sensor with a Fano resonance (FR) response was designed. This sensor topology is demonstrated in Fig. 4 (c). The sensitivity value was 1820 nm/RIU. The plasmonic sensor proposed in Ref. [125] was designed using a triangular resonator coupled to a plasmonic WG. Fig. 4(d) shows the structure of the sensor designed in Ref. [125]. The performance of the sensor was studied by the finite element method (FEM). Its sensitivity and FoM were 2713 nm/RIU and 52.36 RIU^{-1}, respectively.

As mentioned above, the corners of resonators such as hexagonal, rectangular, and triangular resonators have sharp edges. These edges may be rounded through the fabrication procedure. Accordingly, such resonators require high fabrication accuracy. On the other hand, another type of resonator such as a disk resonator that does not have this problem has only one design parameter which is the radius of the disk resonator, and this restricts the designers from realizing an optimal construction. Consequently, one of the best options that does not have the mentioned limitations is the elliptical resonator. Due to the rounded corners of such a resonator and two design parameters of the major radius and the minor radius of the elliptical resonator, it was used to design an RIS [126]. Fig. 4(e) shows the designed sensor configuration. As seen, the proposed sensor structure consists of an elliptical resonator, a straight MIM WG, and a silicon layer. The FDTD simulations of the proposed sensor showed that it generated a multi-resonance mode transmission spectrum. The resonance wavelengths had a red shift by inserting an analyte inside the elliptical resonator. It is because its RI was changed. The FDTD simulations showed that the highest FoM and sensitivity values for the resonance wavelength of 592 nm were 282.5 RIU^{-1} and 550 nm/RIU, respectively.

Using ring-shaped resonators is another technique to design a plasmonic sensor that was used in Ref. [102] (Fig. 4(f)). Such a topology is composed of a ring-shaped resonator and two insulator WGs, etched on a metallic substrate. The proposed structure in Ref. [127] generated two transmission peaks in the range of 400–2500 nm, which made the suggested topology a strong option for significant sensing applications. The strong coupling ability between the filled ring-shaped resonator and MIM WGs results in high transmission efficiency (95 %), sensitivity (1496 nm/RIU), and FoM (104 RIU^{-1}) values.

An additional kind of resonator used in various plasmonic topologies is the stub resonator. In Ref. [128], an MIM WG coupled to a pair of stub resonators was utilized to design a RI plasmonic sensor. Fig. 4(g) shows this sensor structure. The FDTD simulations showed that the proposed topology generated an FR that is an appropriate candidate for the implementation of sensors due to its sharp edge and high sensitivity to RI variations. The ability to use the transmission line method (TLM) for the design and analysis of such a resonator is its main benefit compared to the other resonators. It is because the TLM is several orders of magnitude faster than the other usual methods such as FDTD and FEM.

Ring resonator-based structures, which can be based on different ring types, are another category widely used to design plasmonic sensors [129–131]. Such a structure has several advantages which are desirable for designing optical sensors. For example, this configuration has two distinct output ports, and it can produce high Q-factor resonance modes. Furthermore, since the locations of the resonance modes depend on the integer fractions of the circumference of the ring, depending on the sensor's application, it is possible to adjust the resonance wavelengths by determining a suitable value for the circumference of the ring. Fig. 4(h), (i), and (j) show the plasmonic sensors based on ring resonator-based structures using disk, square, and hexagonal rings, respectively. In Ref. [129], the FDTD results showed a multi-resonance transmission spectrum with the highest sensitivity value of 921 nm/RIU was achieved. The sensor structure designed in Ref. [130] was used for water glucose sensing. In this structure, the sensitivity and FoM values of 6400 nm/RIU and 10000 RIU^{-1} were obtained, respectively for the produced FR. Finally, the last ring resonator-based structure which is used a hexagonal ring [131] produced a single-mode transmission spectrum with a high sensitivity of 4270 nm/RIU.

3.2. Plasmonic sensors based on coupled-resonator structures

Another prevalent method for designing plasmonic sensors with high sensitivities is realized by coupling more than one resonator in the conventional basic platforms. Coupled resonators may have similar or different geometric structures. Coupling resonators together is a well-known method that can increase the sharpness of resonance transition edges. Therefore, such a method can be used to design sensors with higher sensitivities compared to the first technique. In addition to this application, it can also be used for other

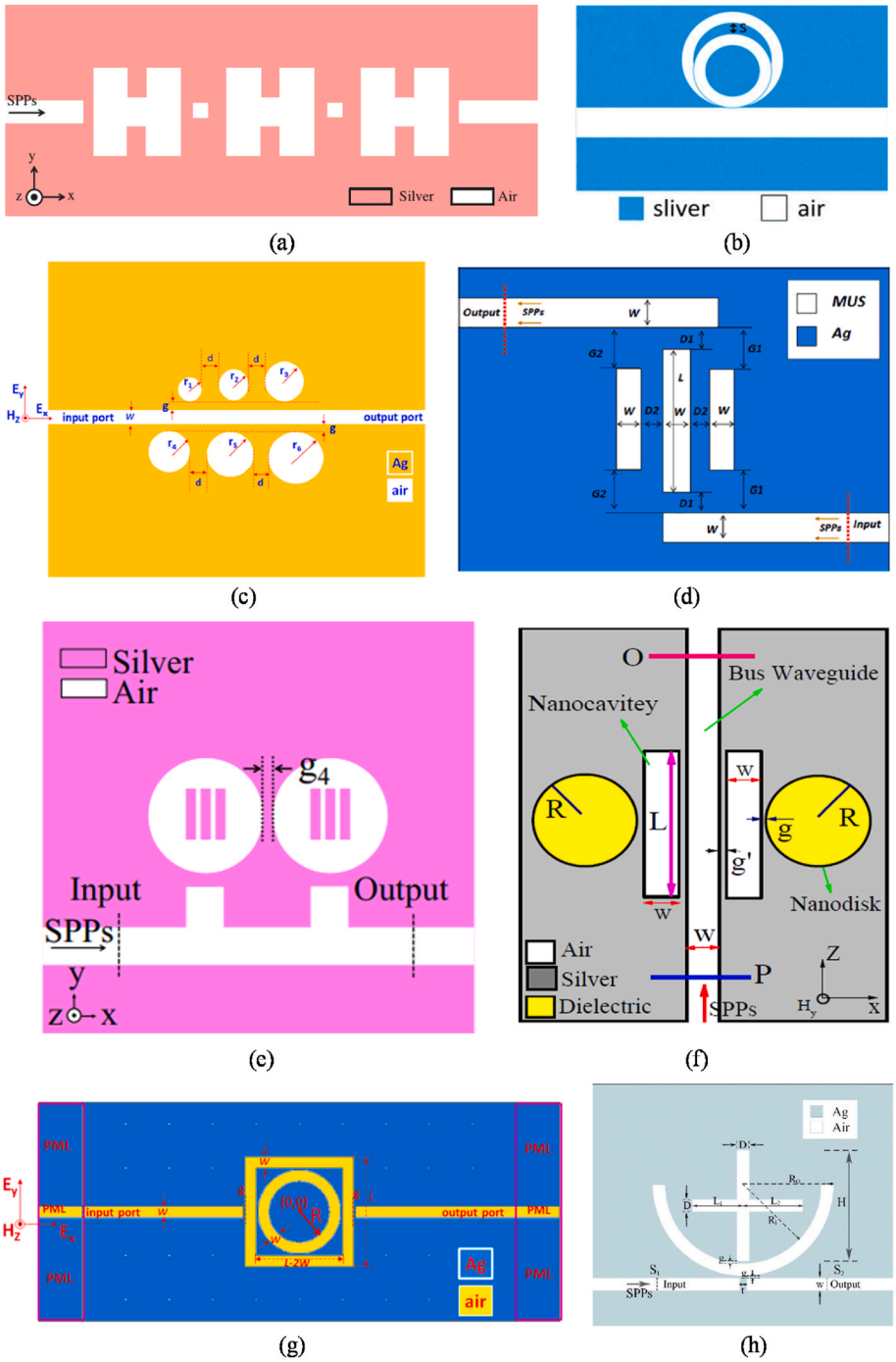

Fig. 5. Examples of plasmonic sensors based on the coupled-resonator structures: (a) H-shaped resonators [132], (b) Ring-shaped resonators [133], (c) Disk resonators [134], (d) Rectangular resonators [135], (e) Disk and stub resonators [136], (f) Disk and rectangular resonators [137], (g) Square ring-shaped and disk ring-shaped resonators [138], (h) Semi-circle ring-shaped and cross-shaped resonators [139].

requests like designing slow-light WGs. Some various works that have used the coupled resonators technique for plasmonic sensor design are reviewed in the following.

In [132], a plasmonic RIS consisting of three coupled H-shaped resonators and two MIM WGs was proposed. Fig. 5(a) shows this structure. The RIS designed in this paper had a single-mode spectrum in a relatively wide wavelength range. One of the main advantages of this work is that to obtain different FoM values, it can be easily redesigned with various units of H-shaped resonators without causing a disturbance in its single-mode response. The sensitivity and FoM of this design were 1050 nm/RIU, and 108.36 RIU^{-1}, respectively. Ref. [133] suggested an RIS using coupled tangent-ring resonators and an MIM WG. The performance of this RIS was investigated with different numbers (two, three, four, five, and six) of tangent-ring resonators. The FDTD results showed that by using two coupled resonators (sensor structure in Fig. 5(b)), there was an FR with an asymmetrical line shape in the transmittance, and the sensitivity and FoM values were 880 nm/RIU and 964 RIU^{-1}, respectively. When the number of resonators was increased, multiple FRs with ultra-sharp edges were generated that could increase the FoM value.

In another work [134], six circular coupled resonators with different radii coupled to an MIM WG from the top and bottom sides were used to design a surface plasmon-based structure for sensing (Fig. 5(c)). The transmittance of this design which was obtained using the FEM had multi-narrowband resonance modes. It is worth mentioning that the maximum sensitivity and FoM of this sensor were 700 nm/RIU and 350 RIU^{-1}, respectively. The other plasmonic sensor structure that will be reviewed in this work is used for temperature and blood group detection [135]. The sensor was designed using three coupled quadrilateral resonators sandwiched perpendicularly between two MIM WGs (Fig. 5(d)). The FEM was used for numerical investigations of this design and an optimization technique was also applied to rectify the performance of the sensor. A sensitivity of 1556 nm/RIU and a FoM of 14.83 nm/RIU were attained for this structure, and when it was used for temperature sensing, a sensitivity of 0.61 nm/°C was achieved.

The next plasmonic RISs reviewed in this work are based on coupled resonators with different geometric structures [136–139]. In Ref. [136], four plasmonic RISs based on stub resonators coupled to disk resonators comprising silver strips and an MIM WG were designed (Fig. 5(e)). Coupling these two types of resonators led to narrow plasmon-induced transparency resonance peaks. In other words, from the interaction between the broad continuous spectrum of the stub resonators and the narrow discrete resonance of the disk resonators containing metal strips, PIT resonance peaks were created. By using a stub resonator coupled to a disk resonator containing metal strips, the initial sensor was proposed. The other three were designed based on two stubs and one disk containing

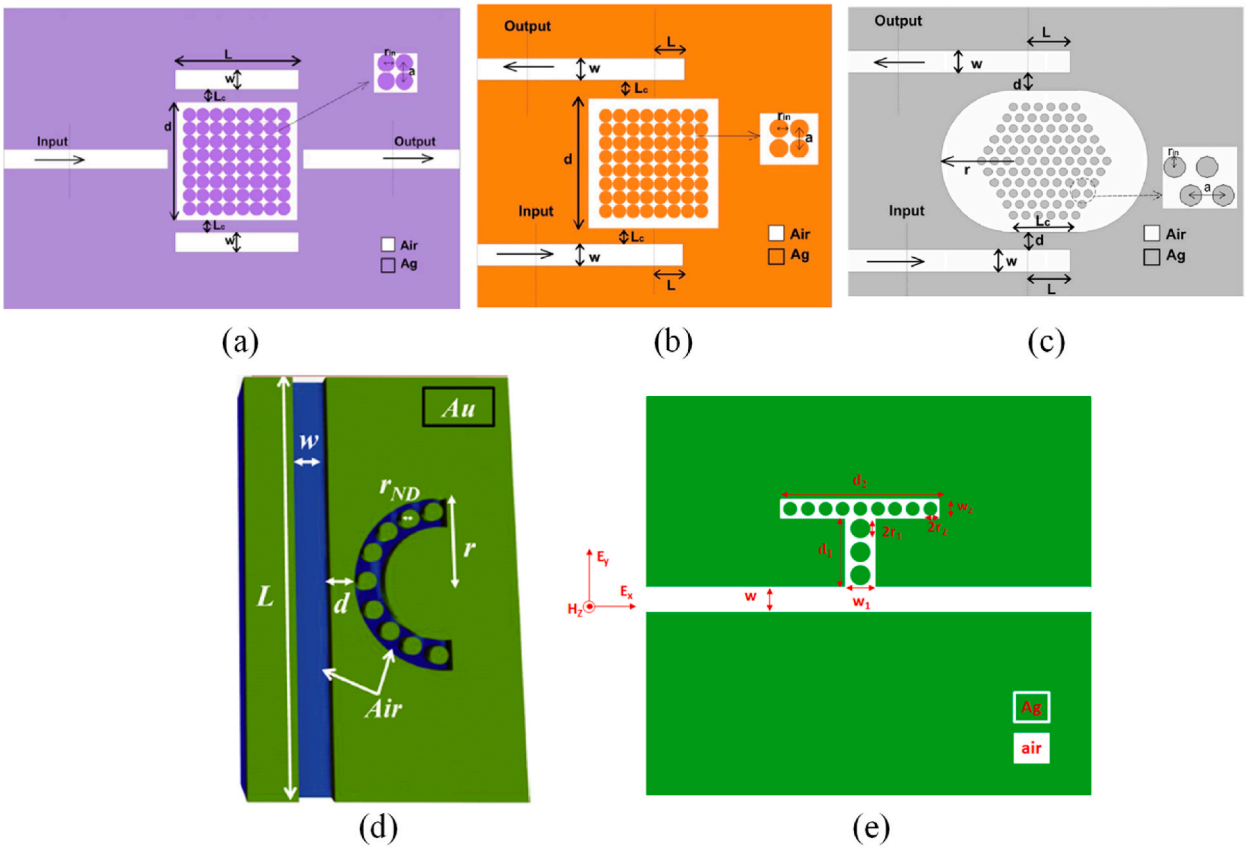

Fig. 6. Examples of plasmonic sensors based on the MI periodic structures: (a) Metal nano-rods in a square resonator coupled to rectangular resonators [140], (b) Metal nano-rods in a square resonator [141], (c) Metal nano-rods in an elliptical resonator [142], (d) Metal nano-rods in a semi-circle ring-shaped resonator [143], (e) Metal nano-rods in a T-shaped resonator [144].

metal strips, one stub and two disks containing metal strips, and two stubs and two disks containing metal strips, respectively. The FDTD results showed that the maximum sensitivities of 725.1, 715.1, 772, and 703.26 nm/RIU and the maximum FoM values of 91.78, 120.18, 144.27, and 113.07 RIU^{-1} were attained for the first to the fourth RISs, respectively.

Fig. 5(f) shows that the next structure reported in Ref. [137] (a tunable plasmonic RIS) used coupled disk and rectangular resonators. The performance characteristics of this design were obtained using the FDTD method. The appearance of a narrow PIT resonance peak for this structure led to high FoM and sensitivity values of 61.55 RIU^{-1} and 800 nm/RIU, respectively. By using the central coupled circular and rectangular ring-shaped resonators, another RIS with a multiple resonance spectrum was designed [138]. Fig. 5(g) shows the total structure of this design. Furthermore, to improve the proposed sensor's sensitivity, several silver baffles were inserted in the rectangular ring-shaped resonator. This enhances the sensitivity by 1.36 times. The FEM results showed that the sensitivity is 3400 nm/RIU and the FoM is 36 RIU^{-1} for the optimized structure (sensor with the silver baffles inserted in the rectangular ring-shaped resonator).

Fig. 5(h) shows the last structure reviewed in this section. As seen, this sensor construction is composed of coupled semi-circle ring-shaped and cross-shaped resonators which were coupled to an MIM WG. The transmission spectrum of this structure had one Lorentz peak and five FRs. In fact, the coupling of continuous states created via the direct WG into the semi-circle resonator and discrete states created in the crosswise resonator generated this spectrum. The suggested RIS in this paper was simulated using the FEM. The sensitivity and FoM values were obtained at 1600 nm/RIU and 193 RIU^{-1}, respectively.

3.3. Plasmonic sensors based on periodic structures

One of the main drawbacks of the second method (coupled-resonator structures) for designing plasmonic sensors is that the size of the structure increases by coupling resonators together, which is not desirable. This is because having a compact size is one of the important factors in designing plasmonic sensors. Accordingly, another method that uses periodic structures has also been used to design plasmonic sensors. Using this method not only improves the performance of the sensors by sharpening the resonance peaks but

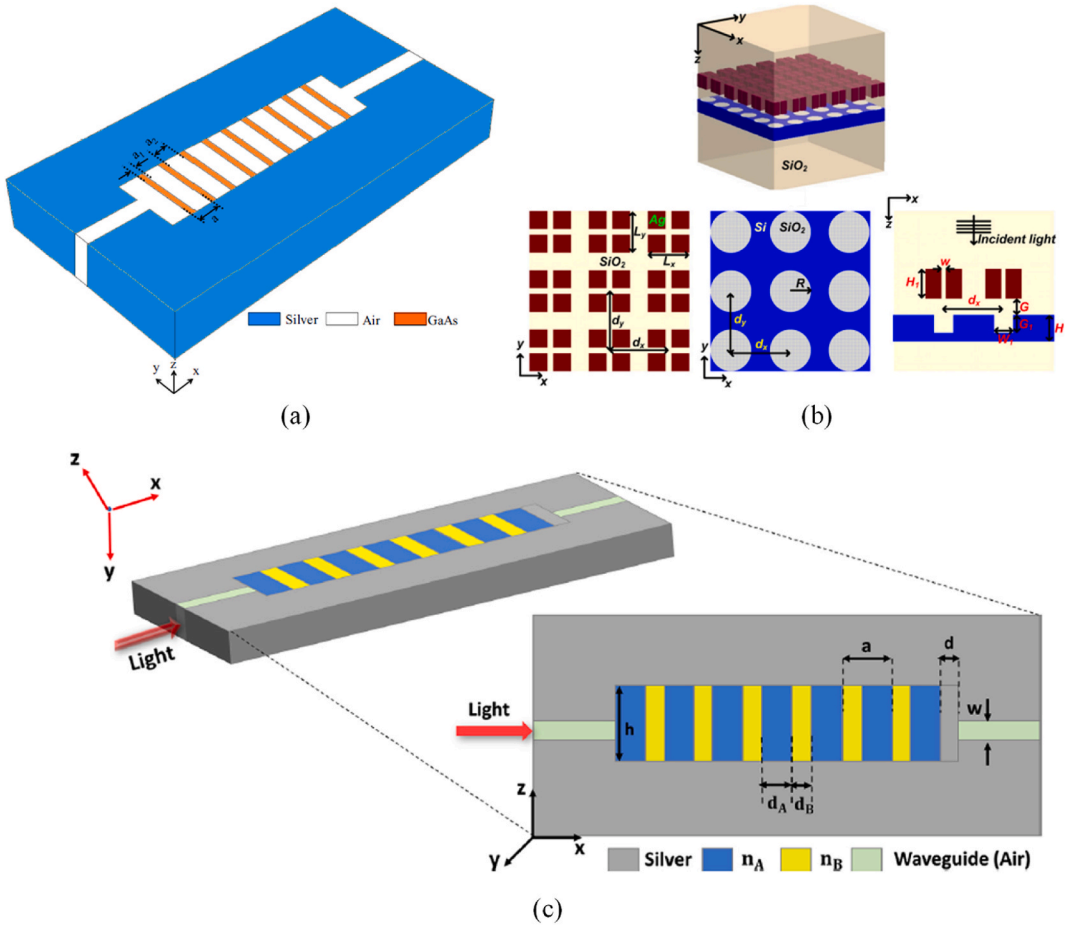

Fig. 7. Examples of plasmonic sensors based on the II periodic structures: (a) Periodic insulator layers [145], (b) Cross-slit metallic photonic crystals and insulator photonic crystals [146], (c) Periodic insulator layers coupled to a metal layer [147].

also reduces the size of the structures compared to the second method. This technique includes two sub-categories, namely MI and II periodic structures that are reviewed in the following.

3.3.1. *Plasmonic sensors based on MI periodic structures*

As mentioned, there are a lot of published works that used periodic MI topologies to progress the performance of plasmonic sensors. Some of such sensor structures are reviewed in this sub-section [116–120]. These structures can be designed by introducing the metal rod defects inside the insulator medium. The placement of these metal rod defects may be in different ways. For example, these periodic arrays can be inserted with square [140,141], triangular [142], irregular [143,144], or other patterns. Also, these defects may have the same [140–143] or different [144] dimensions.

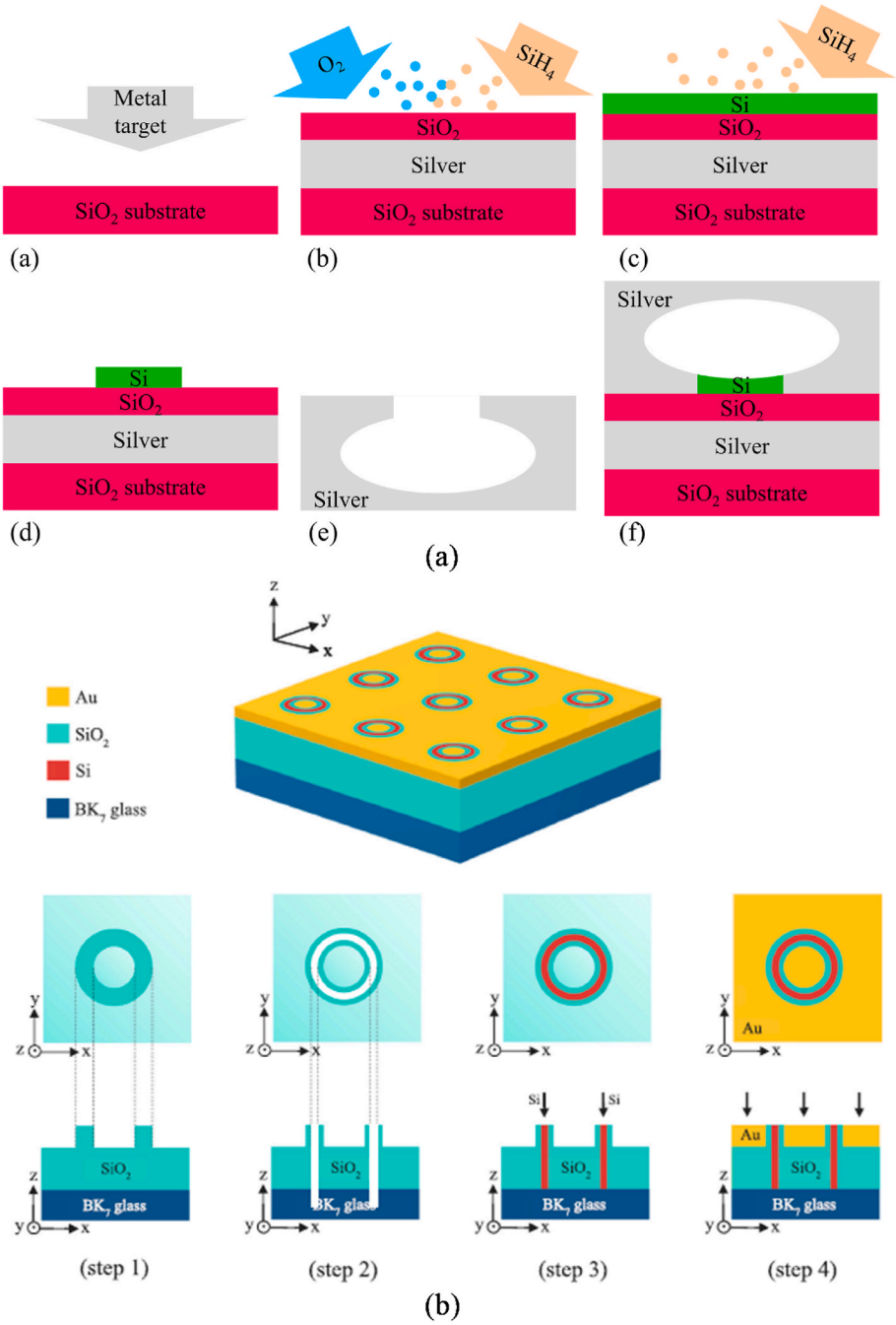

Fig. 8. Fabrication steps of proposed sensors reported in (a) [126], (b) [148].

Fig. 6(a) shows that a tunable sensor structure using a metal rod array inserted in a square resonator coupled to two rectangular resonators and two MIM WGs was designed for glucose concentration monitoring [140]. It is worth saying that both methods of coupled-resonator structures and periodic MI structures were used in this topology. In other words, the suggested design benefited from the advantages of both techniques. The FDTD simulations showed that a sensitivity of 892 nm/RIU was achieved for the suggested sensor.

In [141,142], two compact RISs for temperature sensing based on square and elliptical resonators incorporating periodic metal rod defects and MIM WGs were proposed, respectively (Fig. 6(b) and (c)). Their sensing performance was numerically analyzed by the FDTD method. These two sensor structures had Lorentzian (bell-shaped) frequency responses. The RI and temperature sensitivities of designed sensors in Refs. [141,142] were 2320 nm/RIU, 2610 nm/RIU, 0.84 nm/$^{\circ}$C, and 1.03 nm/$^{\circ}$C, respectively.

The next sensor structure designed based on a semi-circle ring-shaped resonator loaded with periodic metal rod defects coupled to an MIM WG was proposed in Ref. [143]. The suggested sensor is illustrated in Fig. 6(d). To study the effect of metal rod defects, the transmittances of the main sensor and the sensor without defects were compared via the numerical method used in this paper (FEM). As expected, and discussed, the metal rod defects increased the sensitivity significantly. The obtained sensitivity was equal to 1084.21 nm/RIU. The RIS designed in this paper had the ability to be used for biochemical sensing applications.

Fig. 6(e) shows a plasmonic RIS consisting of a T-shaped resonator loaded with metal rods periodically coupled to an MIM WG [144]. Using the metal rods in the T-shaped resonator proposed in this paper could achieve an ultra-high sensitivity value compared to traditional T-shaped resonators. The sensitivity was 8280 nm/RIU. Furthermore, the performance of the suggested RIS was investigated for temperature sensing, and it had a relatively high-temperature sensitivity of about 3.3 nm/$^{\circ}$C for temperature sensing.

3.3.2. Plasmonic sensors based on II periodic structures

Owing to the actuality that metals have inherent losses that cause decreases in the amount of transmission in the frequency response, another method used in some works was II periodic structures. In other words, a combination of plasmonic and PC structures was used in such structures [145–147]. Periodic PC topologies can produce PBGs with sharp edges. This feature is a suitable option to design RISs. In Ref. [145], a periodic one-dimensional II structure (one-dimensional PC lattice) coupled to two MIM WGs was utilized to create a sensor for basal cell cancer detection (Fig. 7(a)). Its transmittance produced a PBG with a wide gap between two sharp edges. This option led to a wide practical wavelength range for the suggested sensor. The sensitivity and FoM of this design sensor using the FDTD method were 718.6 nm/RIU and 156.217 RIU^{-1}, respectively.

Fig. 7(b) shows another sensor structure [146]. As seen, this topology was composed of two periodic structures in a background of SiO_2 material. The top periodic layer was a cross-slit metallic PC structure, and the bottom periodic layer was an II periodic structure (two-dimensional PC lattice). The FDTD simulations showed that due to the coupling effect between the excited WG mode and surface plasmonic mode supported by metallic and insulator PCs, the proposed structure achieved an electromagnetically induced transparency phenomenon with a sensitivity value of 700 nm/RIU.

Finally, the last sensor reviewed in this paper is demonstrated in Fig. 7(c) [147]. The proposed RIS was composed of an II periodic structure (one-dimensional PC lattice) coupled to a metal layer at the end of the PC lattice and two MIM WGs. The numerical FDTD method was applied to design the suggested sensor, and this showed that the transmission spectrum generated two Lorentzian resonance peaks with narrow bandwidths which were suitable for sensing applications. The narrower peak with a bandwidth of 14 nm had an RI sensitivity of 1210 nm/RIU.

4. Fabrication technology of different types of plasmonic sensors

After introducing and studying all category types of plasmonic sensors including conventional basic platforms, coupled resonator structures, and periodic structures, their fabrication technologies are briefly discussed and compared to each other in this section. In the previous sections, it is explained that sensor structures designed using coupled resonators and periodic structures can have higher sensitivity and FoM values than the first category (sensors based on conventional basic platforms). This is because 2-s categories can produce sharper transmission spectra. As known, there is a trade-off between different designing parameters of a sensor. It means that although 2-s categories (coupled resonator and periodic structures) can produce sensors with higher sensitivity and FoM values than the first one (conventional basic platforms), they have a more difficult fabrication procedure due to their more complex structure. Also, regarding the comparison of the fabrication process of the second and third categories, it can be said that periodic structures have far more complicated fabrication procedures than coupled structures.

To create a better view, the fabrication steps of a sensor based on conventional basic platforms [126] and a sensor based on periodic structures [148] are shown in Fig. 8. In the following, detailed explanations of the fabrication steps of both structures (Fig. 8 (a) and (b)) are given. To fabricate the sensor structure proposed in Ref. [126] (Fig. 8 (a)), first, by sputtering, the metal is deposited on the oxide substrate. In the second and third steps, the Silicon dioxide and Silicon layers are grown by chemical vapor deposition, respectively. Thereafter, the Silicon layer is etched. In the two final steps, the cavity shape is etched into the silver layer, and this layer is flipped and attached to the lower section.

Fig. 8 (b) shows the fabrication steps of a unit cell of the sensor structure designed in Ref. [148]. As seen, first, the Silicon dioxide is deposed, and the Silicon dioxide ring pattern is generated on the substrate layer. After that, in steps 3 and 4, the shown part of the Silicon dioxide ring is etched and filled with the Silicon layer, respectively. In the last step, the gold layer is deposited.

As seen in this figure, compared to the size of the proposed resonator in Ref. [126], the dimensions of ring Si and SiO_2 resonators in Ref. [148] are very small. On the other hand, the proposed structure in Ref. [148] is composed of several unit cells which consist of these two coupled ring resonators and it is needed to fabricate all unit cells next to each other. Therefore, this complicated process

needs a much higher fabrication accuracy compared to the structure proposed in Ref. [126].

5. Performance comparison of the reported plasmonic sensors in the literature

In this section, to give a general view of the reported plasmonic sensors' performance, their main features are summarized in some comparison tables. These properties are the topology type of the sensors designed in the literature, the used material, the simulation method, the spectrum type of their transmission spectrum, the sensitivity, the FoM, and the total footprint of the sensor structures.

Table 1
Performance comparison of the suggested plasmonic sensors reported in the literature.

Category	Ref.	Topology	Material	Simulation method	Spectrum	Sensitivity (nm/RIU)	FoM (RIU^{-1})	Size (nm^2)
Conventional basic platforms	[122]	A disk resonator and two MIM WGs	Air, Ag	FDTD	Lorentzian	357.1	–	400 × 840
	[123]	A hexagonal resonator and one MIM WG	Air, Ag, Dielectric	FDTD	Lorentzian	1562.5	38.6	900 × 1300
	[124]	A rectangular resonator and two MIM WGs	Air, Ag	FEM	Fano	1820	–	110 × 950
	[125]	A triangular resonator and one MIM WG	Air, Ag, Dielectric	FEM	Lorentzian	2713	52.36	688 × 910
	[126]	An elliptical resonator and one MIM WG	Air, Ag, Si, SiO_2	FDTD	Lorentzian	550	282.5	460 × 1200
	[127]	A rectangular ring-shaped resonator and two MIM WGs	Si, Ag, Dielectric	FEM	Lorentzian	1496	104	350 × 810
	[128]	Two stub resonators and one MIM WG	Air, Ag	FDTD	Fano	–	–	500 × 737
	[129]	A disk ring resonator and two MIM WGs	Air, Ag	FDTD	Lorentzian	921	–	812 × 1100
	[130]	A rectangular ring resonator and two MIM WGs	Air, Ag	FDTD	Fano	6400	10000	510 × 580
	[131]	A hexagonal ring resonator and two MIM WGs	Air, Ag	FDTD	Lorentzian	4270	–	510 × 580
Coupled-resonator structures	[132]	Three H-shaped resonators and two MIM WGs	Air, Ag	FDTD	Lorentzian	1050	108.36	270 × 1380
	[133]	Two tangent-ring resonators and one MIM WG	Air, Ag	FDTD	Fano	880	964	170 × 520
	[134]	Six disk resonators and one MIM WG	Air, Ag	FEM	Lorentzian	700	350	640 × 1464
	[135]	Three rectangular resonators and two MIM WGs	Air, Ag	FEM	Lorentzian	1556	14.83	550 × 720
	[136]	two stubs and two disks containing metal strips and one MIM WG	Air, Ag	FDTD	PIT	703.26	113.07	530 × 970
	[137]	Two disk and two rectangular resonators and one MIM WG	Air, Ag, Dielectric	FDTD	PIT	800	61.55	900 × 1010
	[138]	One square and one disk ring-shaped resonator and two MIM WGs	Air, Ag	FEM	Lorentzian	3400	36	500 × 920
	[139]	One semi-circle ring-shaped and one cross-shaped resonator and one MIM WG	Air, Ag	FEM	Fano and Lorentzian	1600	193	570 × 1140
Periodic MI structures	[140]	One square resonator with metal rods and two rectangular resonators and two MIM WGs	Air, Ag	FDTD	Lorentzian	892	–	510 × 810
	[141]	One square resonator with metal rods and two MIM WGs	Air, Ag	FDTD	Lorentzian	2320	–	510 × 580
	[142]	One elliptical resonator with metal rods and two MIM WGs	Air, Ag	FDTD	Lorentzian	2610	–	510 × 700
	[143]	One semi-circle ring-shaped with metal rods and one MIM WG	Air, Ag	FEM	Lorentzian	1084.21	–	400 × 1000
	[144]	One T-shaped resonator with metal rods and one MIM WG	Air, Ag	FEM	Lorentzian	8280	–	230 × 730
Periodic II structures	[145]	One-dimensional PC and two MIM WGs	Air, Ag, GaAs	FDTD	PBG	718.6	156.217	250 × 4380
	[146]	One cross slit metallic PC structure and two-dimensional PC	Si, Ag, AiO_2	FDTD	Lorentzian	700	–	760 × 760
	[147]	One dimensional PC coupled to a metal layer and two MIM WGs	Air, Ag, Insulator with $n_1 = 1.4$	FDTD	Lorentzian	1210	–	250 × 950

Tables 1 and 2 present these parameters. Also, the applications, detection ranges, and publication year of reported sensors, are given in Table 3. As seen in Table 1, based on the topology types and material of the designed sensors, different spectra types with various sensitivities and FoM values were achieved. Accordingly, the results collected in this review paper can give a suitable perspective for optical sensors based on plasmonic structures that will be designed in the future.

As seen in Tables 1 and in most works, Ag and air have been used as metal and insulator materials to design the sensors. The reason for this can be explained as follows. Since noble metals such as Ag and Au have large negative real parts and small imaginary parts of permittivity in terahertz frequencies, they are usually utilized in plasmonic sensors. On the other hand, among these two noble metals, Au is more expensive than Ag, which has made Ag more widely used than Au. Also, because air is an available insulator material and can easily be replaced with other insulators in the plasmonic sensor structures, it is the most widely used insulator material in plasmonic sensors.

Since other structures have been designed and presented using different metals and insulators, we report the performance of some of them in a separate table (Table 2) to have a more comprehensive study. As shown in Table 2, the comparison parameters of these works are the same as in Table 1.

As discussed before, sensors have different applications in various fields such as chemistry, physics, and biomedical. All the sensors reported in the literature are sensitive to changes in the refractive index of their analyte. Hence, all of them are generally designed and presented as refractive index sensors. But in some works, special applications for designed sensors are presented. These applications and the detection wavelength ranges of sensors are reported in Table 3.

6. Discussions on the future of plasmonic sensors

As discussed, plasmonic sensors have some advantages such as their small footprints (nanometer-scale), high sensitivity, and flexibility. As a result, these properties motivate researchers to design and propose various surface plasmon-based sensors based on different structure types. However, there is still a demand for plasmonic sensors with higher performance. Therefore, this section is devoted to the future perspective for designing plasmonic sensors by overcoming the existing limitations.

The most important current challenge is increasing the sensitivity, FOM, and resolution of plasmonic sensors. Research shows that combining two-dimensional nanomaterials with noble metals plays a significant role in developing sensor performance parameters such as sensitivity, FOM, and detection accuracy. Two-dimensional nanomaterials such as graphene, black phosphorus, MXenes, and dichalcogenide of transition metals significantly improve performance parameters and protect metal layers against oxidation. This is because adding a two-dimensional nanomaterial layer raises the electrical field at the interface and accelerates the transfer of charges between plasmonic metal and probe molecules due to the high mobility of the carrier, thereby enhancing the sensitivity of the surface plasmon-based sensors. Also, it is worth mentioning that emerging quantum plasmonics present a new paradigm shift in optical sensing from classical measurement to quantum metrology, which has realized outstanding performance beyond traditional techniques. Accordingly, more realistic applications in medicine and biochemistry based on quantum technology are anticipated shortly. However, the research on two-dimensional nanomaterials and quantum sensing is still in its initial stages, and as a very attractive field of science and technology, it needs more research.

7. Conclusion

In this review, surface plasmon-based optical sensors reported in the literature are studied. According to the structures used in different papers, here, such sensors are divided into three general groups. The first category is based on conventional basic platforms which include a resonator coupled to two WGs from both sides, a resonator coupled to a WG from one side, and a ring resonator-based structure. The second group is coupled-resonator structures, and the last one is periodic structures. The third method includes two kinds of MI and II periodic structures. Finally, the performance of such sensors is reviewed and compared to each other based on their topology types, transmission spectrum types, and their main characteristics such as sensitivity and FoM parameters.

Table 2
Performance comparison of the plasmonic sensors with different metal and insulator materials from the reported sensors in Table 1.

Ref.	Topology	Material	Simulation method	Spectrum	Sensitivity (nm/RIU)	FoM (RIU^{-1})	Size (nm^2)
[149]	Triplet-coupled stub resonators, a disk resonator and one MIM waveguide	Insulaor, Ag	FDTD	Fano	684	621.8	1190 × 1200
[150]	A gold spiral resonator inside a rod-type hexagonal Si PhC caviy	Si, Au	FDTD	Lorentzian	1675	2991	16770 × 19350
[151]	An 8-shaped resonator and two MIM waveguides	Insulaor, Ag	FDTD	Lorentzian	1200	–	675 × 680
[152]	An FK51A prism, thin metal film, 8 nm $BaTiO_3$, 3 layers of BlueP/MoS_2 hetero-structure, and a sensing medium	Blue P/MoS_2, $BaTiO_3$, Ag	FDTD	Lorentzian	347.82	–	–
[153]	A rod-type PhC structure and some metallic rods	Si, SiO_2, Ag	FDTD	PBG	1672	2388	–
[154]	A hybrid layer of gold-zinc oxide	ZnO-Au	FDTD	Lorentzian	–	–	–

Table 3
Applications of the plasmonic sensors reported in the literature.

Category	Ref.	Application	Detection range (RI)	Year
Conventional basic platforms	[122]	Sensing RI of material under sensing	1–1.5	2013
	[123]	Sensing RI of material under sensing	1–1.12	2015
	[124]	Sensing RI of material under sensing	1–1.1	2016
	[125]	Biomedical applications	1–1.4	2021
	[126]	Sensing RI of material under sensing	1–1.34	2021
	[127]	Biomedical applications	1–1.5	2016
	[128]	Sensing RI of material under sensing	1–1.06	2017
	[129]	Sensing RI of material under sensing	1–1.05	2015
	[130]	Glucose concentration sensing	1–1.05	2019
	[131]	Sensing RI of material under sensing	1–1.2	2016
Coupled-resonator structures	[132]	Sensing RI of material under sensing	1–1.01	2022
	[133]	Sensing RI of material under sensing	1–1.1	2018
	[134]	Inspecting hemoglobin concentration in human blood samples	1–1.03	2021
	[135]	Temperature and blood group detection	1.4–1.5	2020
	[136]	Sensing RI of material under sensing	1–1.04	2023
	[137]	Sensing RI of material under sensing	1–1.04	2020
	[138]	Sensing RI of material under sensing	1–1.15	2021
	[139]	Sensing RI of material under sensing	1–1.08	2020
Periodic MI structures	[140]	Glucose concentration monitoring	1–1.15	2018
	[141]	Human blood group identification	1–1.1	2017
	[142]	Sensing RI of material under sensing	1–1.05	2017
	[143]	Biomedical sensing applications	1–1.38	2020
	[144]	Sensing RI of material under sensing	1–1.5	2019
Periodic II structures	[145]	Detection of basal cell cancer	1–1.005	2022
	[146]	Sensing RI of material under sensing	1.3–1.7	2011
	[147]	Sensing RI of material under sensing	1–1.6	2021
Structures with different materials	[149]	Sensing RI of material under sensing	1–1.05	2023
	[150]	Detection of various blood components	1.33–1.4	2024
	[151]	Detection of basal cancer cells	1.36–1.38	2023
	[152]	Sensing medium with refractive indices up to 1.335	1.33–1.35	2021
	[153]	Sensing RI of material under sensing	1.33–1.34	2022
	[154]	Hyperuricemia detection	–	2023

CRediT authorship contribution statement

Shiva Khani: Writing – review & editing, Writing – original draft, Resources, Methodology, Investigation. **Pejman Rezaei:** Writing – review & editing.

Data availability

No data was used for the research described in the article.

Declaration of competing interest

The authors declare that they have no known competing financial interests or personal relationships that could have appeared to influence the work reported in this paper.

Acknowledgments

This work was supported by Semnan University. The authors would also like to thank the editor and respected reviewers for their valuable comments.

References

[1] I.C. Cherik, S. Mohammadi, Vertical tunneling field-effect transistor with germanium source and T-shaped silicon channel for switching and biosensing applications: a simulation study, IEEE Trans. Electron. Dev. 69 (9) (2022) 5170–5176.
[2] S. Khani, M. Hayati, Compact microstrip lowpass filter with wide stopband and sharp roll-off, Microw. J. 60 (11) (2017) 86–92.
[3] I.C. Cherik, S. Mohammadi, Dielectric modulated doping-less tunnel field-effect transistor, a novel biosensor based on cladding layer concept, IEEE Sensor. J. 22 (11) (2022) 10308–10314.
[4] F.J. Ferrández-Pastor, J.M. García-Chamizo, M. Nieto-Hidalgo, Electromagnetic differential measuring method: application in microstrip sensors developing, Sensors 17 (7) (2017) 1650.
[5] S. Khani, S.V.A.D. Makki, S.M.H. Mousavi, M. Danaie, P. Rezaei, Adjustable compact dual-band microstrip bandpass filter using T-shaped resonators, Microw. Opt. Technol. Lett. 59 (12) (2017) 2970–2975.
[6] M. Navaei, P. Rezaei, S. Kiani, Measurement of low-loss aqueous solutions permittivity with high detection accuracy by a contact and free-label resonance microwave sensor, Int. J. Commun. Syst. 36 (5) (2023) e5417.

[7] M. Ebnali-Heidari, H. Saghaei, F. Koohi-Kamali, M.N. Moghadasi, M.K. Moravvej-Farshi, Proposal for supercontinuum generation by optofluidic infiltrated photonic crystal fibers, IEEE J. Sel. Top. Quant. Electron. 20 (5) (2014) 582–589.
[8] A. Tavousi, M.R. Rakhshani, M.A. Mansouri-Birjandi, High sensitivity label-free refractometer based biosensor applicable to glycated hemoglobin detection in human blood using all-circular photonic crystal ring resonators, Opt Commun. 429 (2018) 166–174.
[9] L. Li, J. Xu, J. Li, X. Lyu, Z. Liu, J. Wei, Redox responsive photonic crystals with broad wavelength shifts and their efficient detection of hydrogen peroxide and catalase, Sensor. Actuator. B Chem. 373 (2022) 132721.
[10] S. Armaghani, S. Khani, M. Danaie, Design of all-optical graphene switches based on a Mach-Zehnder interferometer employing optical Kerr effect, Superlattice. Microst. 135 (2019) 106244.
[11] A. Farmani, A. Mir, M. Irannejad, 2D-FDTD simulation of ultra-compact multifunctional logic gates with nonlinear photonic crystal, JOSA B 36 (4) (2019) 811–818.
[12] V.S. Chaudhary, D. Kumar, B.P. Pandey, S. Kumar, Advances in photonic crystal fiber-based sensor for detection of physical and biochemical parameters-A review, IEEE Sensor. J. 23 (2) (2022) 1012–1023.
[13] Q. Li, S. Liu, J. Wang, N.M. Mbola, Z. Meng, X. Wang, M. Xue, A biocompatible, self-adhesive, and stretchable photonic crystal sensor for underwater motion detection, J. Mater. Chem. C 10 (23) (2022) 9025–9034.
[14] N.A. Mohammed, O.E. Khedr, E.S.M. El-Rabaie, A.A. Khalaf, Literature review: on-chip photonic crystals and photonic crystal fiber for biosensing and some novel trends, IEEE Access 10 (2022) 47419–47436.
[15] F. Parandin, A. Sheykhian, Design and simulation of a 2× 1 All-Optical multiplexer based on photonic crystals, Opt. Laser Technol. 151 (2022) 108021.
[16] S. Khani, M. Danaie, P. Rezaei, Hybrid all-optical infrared metal-insulator-metal plasmonic switch incorporating photonic crystal bandgap structures, Photon. Nanostruct: Fundam. Appl. 40 (2020) 100802.
[17] M. De, T.K. Gangopadhyay, V.K. Singh, Prospects of photonic crystal fiber as physical sensor: an overview, Sensors 19 (3) (2019) 464.
[18] G. Pitruzzello, T.F. Krauss, Photonic crystal resonances for sensing and imaging, J. Opt. 20 (7) (2018) 073004.
[19] S.E. Abd El-Ghany, W.M. Nouman, Z.S. Matar, Z.A. Zaky, A.H. Aly, Optimized bio-photonic sensor using 1D-photonic crystals as a blood hemoglobin sensor, Phys. Scripta 96 (3) (2020) 035501.
[20] P. Colman, P. Lunnemann, Y. Yu, J. Mørk, Ultrafast coherent dynamics of a photonic crystal all-optical switch, Phys. Rev. Lett. 117 (23) (2016) 233901.
[21] M.R. Jalali Azizpour, M. Soroosh, N. Dalvand, Y. Seifi-Kavian, All-optical ultra-fast graphene-photonic crystal switch, Crystals 9 (9) (2019) 461.
[22] S.P. Yu, D.C. Cole, H. Jung, G.T. Moille, K. Srinivasan, S.B. Papp, Spontaneous pulse formation in edgeless photonic crystal resonators, Nat. Photonics 15 (6) (2021) 461–467.
[23] W. Peng, B. Huang, X. Huang, H. Song, Q. Liao, A flexible and stretchable photonic crystal sensor for biosensing and tactile sensing, Heliyon 8 (11) (2022) e11697.
[24] B. Wang, M.A. Cappelli, A tunable microwave plasma photonic crystal filter, Appl. Phys. Lett. 107 (17) (2015) 171107.
[25] Y. Liu, S. Wang, D. Zhao, W. Zhou, Y. Sun, High quality factor photonic crystal filter at k≈ 0 and its application for refractive index sensing, Opt Express 25 (9) (2017) 10536–10545.
[26] K. Shinoda, Y. Ohtera, M. Hasegawa, Snapshot multispectral polarization imaging using a photonic crystal filter array, Opt Express 26 (12) (2018) 15948–15961.
[27] F. Mehdizadeh, M. Soroosh, A new proposal for eight-channel optical demultiplexer based on photonic crystal resonant cavities, Photonic Netw. Commun. 31 (1) (2016) 65–70.
[28] M.M. Dangi, A.M. Aghdam, R. Karimzadeh, H. Saghaei, Design and simulation of high-quality factor all-optical demultiplexers based on a two-dimensional photonic crystal, Optics Continuum 1 (7) (2022) 1458–1473.
[29] A. Rostami, F. Nazari, H.A. Banaei, A. Bahrami, A novel proposal for DWDM demultiplexer design using modified-T photonic crystal structure, Photon. Nanostruct: Fundam. Appl. 8 (1) (2010) 14–22.
[30] H.L. Chen, S.G. Li, Z.K. Fan, G.W. An, J.S. Li, Y. Han, A novel polarization splitter based on dual-core photonic crystal fiber with a liquid crystal modulation core, IEEE Photon. J. 6 (4) (2014) 1–9.
[31] Y.F. Gao, J.P. Sun, N. Xu, Z. Jiang, Q.C. Hou, H. Song, C. Zhang, Manipulation of topological beam splitter based on honeycomb photonic crystals, Opt Commun. 483 (2021) 126646.
[32] M.K. Moghaddam, A.R. Attari, M.M. Mirsalehi, Improved photonic crystal directional coupler with short length, Photon. Nanostruct: Fundam. Appl. 8 (1) (2010) 47–53.
[33] M.F.O. Hameed, S.S.A. Obayya, K. Al Begain, A.M. Nasr, M.A. El Maaty, Coupling characteristics of a soft glass nematic liquid crystal photonic crystal fibre coupler, IET Optoelectron. 3 (6) (2009) 264–273.
[34] M. Li, J. Ling, Y. He, U.A. Javid, S. Xue, Q. Lin, Lithium niobate photonic-crystal electro-optic modulator, Nat. Commun. 11 (1) (2020) 4123.
[35] Y. Huang, Y. Wang, L. Zhang, Y. Shao, F. Zhang, C. Liao, Y. Wang, Tunable electro-optical modulator based on a photonic crystal fiber selectively filled with liquid crystal, J. Lightwave Technol. 37 (9) (2019) 1903–1908.
[36] H.M. Hussein, T.A. Ali, N.H. Rafat, A review on the techniques for building all-optical photonic crystal logic gates, Opt. Laser Technol. 106 (2018) 385–397.
[37] E. Veisi, M. Seifouri, S. Olyaee, Design and numerical analysis of multifunctional photonic crystal logic gates, Opt. Laser Technol. 151 (2022) 108068.
[38] N.M. D'souza, V. Mathew, Interference based square lattice photonic crystal logic gates working with different wavelengths, Opt. Laser Technol. 80 (2016) 214–219.
[39] G. Marty, S. Combrié, F. Raineri, A. De Rossi, Photonic crystal optical parametric oscillator, Nat. Photonics 15 (1) (2021) 53–58.
[40] S. Khani, M. Danaie, P. Rezaei, Plasmonic all-optical modulator based on the coupling of a surface Plasmon stub-filter and a meandered MIM waveguide, Opt. Quant. Electron. 54 (12) (2022) 1–21, 849.
[41] C.T. Chou Chao, Y.F. Chou Chau, Highly sensitive multichannel Fano resonance-based plasmonic sensor for refractive index and temperature sensing application, Photonics 10 (1) (2023, January) 82. MDPI, 10(1), 82.
[42] S. Khani, A. Farmani, A. Mir, Reconfigurable and scalable 2, 4-and 6-channel plasmonics demultiplexer utilizing symmetrical rectangular resonators containing silver nano-rod defects with FDTD method, Sci. Rep. 11 (1) (2021) 13628.
[43] S.A. Maier, S.A. Maier, Surface plasmon polaritons at metal/insulator interfaces, Plasmon.Fundamentals Appl. (2007) 21–37.
[44] J.A. Dionne, L.A. Sweatlock, M.T. Sheldon, A.P. Alivisatos, H.A. Atwater, Silicon-based plasmonics for on-chip photonics, IEEE J. Sel. Top. Quant. Electron. 16 (1) (2010) 295–306.
[45] A. Farmani, Three-dimensional FDTD analysis of a nanostructured plasmonic sensor in the near-infrared range, JOSA B 36 (2) (2019) 401–407.
[46] S.I. Bozhevolnyi, V.S. Volkov, E. Devaux, J.Y. Laluet, T.W. Ebbesen, Channel plasmon subwavelength waveguide components including interferometers and ring resonators, Nature 440 (7083) (2006) 508–511.
[47] D.K. Gramotnev, S.I. Bozhevolnyi, Plasmonics beyond the diffraction limit, Nat. Photonics 4 (2) (2010) 83–91.
[48] A. Hamouleh-Alipour, S. Khani, M. Ashoorirad, R. Baghbani, Trapped multimodal resonance in magnetic field enhancement and sensitive THz plasmon sensor for toxic materials accusation, IEEE Sensor. J. 23 (13) (2023) 14057–14066.
[49] S.G. Shafagh, H. Kaatuzian, Ultra-high-sensitive plasmonic sensor based on asymmetric hexagonal nano-ring resonator for cancer detection, Heliyon 10 (14) (2024) e34439.
[50] C. Saha, F. Haque, N. Islam, M.M. Hossain, M.E. Arafat, M.A. Yousuf, M.M. Rahman, Dual-Core silver-coated plasmonic sensor modelling with machine learning, Heliyon (2024) e38175.
[51] S.M. Ebadi, S. Khani, Highly-Miniaturized nano-plasmonic filters based on stepped impedance resonators with tunable cut-off wavelengths, Plasmonics 1–12 (8) (2023) 1607–1618.
[52] A. Afroozeh, Numerical and analytical modeling of plasmonic filter with high Q-factor based on "nanostructured resonator", Plasmonics 17 (1) (2022) 371–379.

[53] R. Shafiq, A.D. Khan, F.F. Al-Harbi, F. Ali, A. Armghan, M. Asif, M. Dalarsson, Optical transmission plasmonic color filter with wider color gamut based on X-shaped nanostructure, Photonics 9 (4) (2022) 209.
[54] S. Khani, M. Danaie, P. Rezaei, Tunable single-mode bandpass filter based on metal–insulator–metal plasmonic coupled U-shaped cavities, IET Optoelectron. 13 (4) (2019) 161–171.
[55] Y. Ye, Y. Xie, T. Song, Y. Wang, J. Chai, B. Liu, Y. Liu, Design of a novel plasmonic splitter with variable transmissions and selectable channels, IEEE Trans. Nanotechnol. 18 (2019) 617–625.
[56] X. Shi, W. Yang, H. Xing, X. Chen, Design of power splitters based on hybrid plasmonic waveguides, Appl. Sci. 11 (18) (2021) 8644.
[57] A.E. Kivaj, H. Amanzadeh, Design and simulation of a three-channel plasmonic demultiplexer in an MIM waveguide, Heliyon (2024) e24635.
[58] S. Khani, M. Danaie, P. Rezaei, Double and triple-wavelength plasmonic demultiplexers based on improved circular nanodisk resonators, Opt. Eng. 57 (10) (2018), 107102-107102.
[59] S.M. Ebadi, S. Khani, Design of a tetra-band MIM plasmonic absorber based on triangular arrays in an ultra-compact MIM waveguide, Opt. Quant. Electron. 55 (6) (2023) 482.
[60] S. Swarnakar, S.P.K. Anguluri, S. Kumar, Design and analysis of miniaturized all-optical binary to gray code converter using Y-shaped plasmonic waveguide for optical processors, Photonic Netw. Commun. 44 (1) (2022) 21–29.
[61] S. Khani, M. Danaie, P. Rezaei, Compact and low-power all-optical surface plasmon switches with isolated pump and data waveguides and a rectangular cavity containing nano-silver strips, Superlattice. Microst. 141 (2020) 106481.
[62] X. Zhang, J. Yang, Ultrafast plasmonic optical switching structures and devices, Front. Phy. 7 (2019) 190.
[63] S. Khani, A. Farmani, P. Rezaei, Optical resistance switch for optical sensing, in: Artificial Intelligence in Mechatronics and Civil Engineering: Bridging the Gap, Springer Nature Singapore, Singapore, 2023, pp. 1–38.
[64] J. Dong, M. Wang, Y. Zhou, C. Zhou, Q. Wang, DNA-based adaptive plasmonic logic gates, Angew. Chem. Int. Ed. 59 (35) (2020) 15038–15042.
[65] T. Sadeghi, S. Golmohammadi, A. Farmani, H. Baghban, Improving the performance of nanostructure multifunctional graphene plasmonic logic gates utilizing coupled-mode theory, Appl. Phys. B 125 (2019) 1–12.
[66] M. Deng, X. Wang, J. Chen, Z. Li, M. Xue, Z. Zhou, Z. Fang, Plasmonic modulation of valleytronic emission in two-dimensional transition metal dichalcogenides, Adv. Funct. Mater. 31 (20) (2021) 2010234.
[67] S. Khani, M. Danaie, P. Rezaei, Fano Resonance using surface plasmon polaritons in a nano-disk resonator coupled to perpendicular waveguides for amplitude modulation applications, Plasmonics 16 (6) (2021) 1891–1908.
[68] K. Yang, Y. Chen, S. Yan, W. Yang, Nanostructured surface plasmon resonance sensors: toward narrow linewidths, Heliyon 9 (6) (2023) e16598.
[69] S. Nangare, P. Patil, Black phosphorus nanostructure based highly sensitive and selective surface plasmon resonance sensor for biological and chemical sensing: a review, Crit. Rev. Anal. Chem. 53 (1) (2023) 1–26.
[70] Y.J. Kim, A. Nguyen, G.H. Lee, S. Kim, D.C. Shin, D.H. Kim, S. Kim, Real-time Monitoring of Fast Gas Dynamics with a Single-Molecule Resolution by Frequency-Comb-Referenced Plasmonic Phase Spectroscopy, 2023.
[71] J. Cai, Y. Liu, X. Shu, Long-period fiber grating sensors for chemical and biomedical applications, Sensors 23 (1) (2023) 542.
[72] U.S. Dinish, G. Balasundaram, Y.T. Chang, M. Olivo, Sensitive multiplex detection of serological liver cancer biomarkers using SERS-active photonic crystal fiber probe, J. Biophot. 7 (11-12) (2014) 956–965.
[73] A.K. Sharma, Plasmonic biosensor for detection of hemoglobin concentration in human blood: design considerations, J. Appl. Phys. 114 (4) (2013) 044701.
[74] M.R. Rakhshani, Wide-angle perfect absorber using a 3D nanorod metasurface as a plasmonic sensor for detecting cancerous cells and its tuning with a graphene layer, Photon. Nanostruct: Fundam. Appl. 43 (2021) 100883.
[75] M.A. Butt, R. Piramidowicz, Orthogonal mode couplers for plasmonic chip based on metal–insulator–metal waveguide for temperature sensing application, Sci. Rep. 14 (1) (2024) 3474.
[76] IEEE Standard Letter Designations for Radar-Frequency Bands, IEEE, New York, NY, USA, 1984.
[77] A. Kumar, A.K. Shringi, M. Kumar, RF sputtered CuO anchored SnO2 for H2S gas sensor, Sensor. Actuator. B Chem. 370 (2022) 132417.
[78] B.B. Ngoune, M. Dumon, B. Vignesh, B. Bondu, S. Subbiah, G. Perrin, H. Hallil, Comparison of calibration strategies for a high sensitivity PEI-based RF humidity sensor, IEEE Sensor. J. 24 (8) (2024) 13518–13529.
[79] A. Armghan, T.M. Alanazi, A. Altaf, T. Haq, Characterization of dielectric substrates using dual band microwave sensor, IEEE Access 9 (2021) 62779–62787.
[80] W. Luo, C. Li, L. Wang, L. Qian, D. Li, L. Miao, H. Li, Microwave humidity sensor based on shorted split ring resonator with interdigital capacitance and α-Al2O3 nanoflakes/chitosan sensitive film for respiration monitoring, Sensor. Actuator. B Chem. 413 (2024) 135869.
[81] D. Hambaryan, T. Abrahamyan, H. Parsamyan, A. Movsisyan, B. Minasyan, H. Haroyan, K. Nerkararyan, Dielectric coated conductive rod resonantly coupled with a cut transmission line as a tunable microwave bandstop filter and sensor, Heliyon 10 (2) (2024) e24477.
[82] J. Hasch, E. Topak, R. Schnabel, T. Zwick, R. Weigel, C. Waldschmidt, Millimeter-wave technology for automotive radar sensors in the 77 GHz frequency band, IEEE Trans. Microw. Theor. Tech. 60 (3) (2012) 845–860.
[83] A.W. Raymond, B.J. Drouin, A. Tang, E. Schlecht, E. Mazur, Miniature cavity for in situ millimeter wave gas sensing: N2O and CH3OH detection, Sensor. Actuator. B Chem. 254 (2018) 763–770.
[84] S. Hadipour, P. Rezaei, A graphene-based triple-band THz metamaterial absorber for cancer early detection, Opt. Quant. Electron. 55 (13) (2023) 1122.
[85] P. Zamzam, P. Rezaei, Y.I. Abdulkarim, O.M. Daraei, Graphene-based polarization-insensitive metamaterials with perfect absorption for terahertz biosensing applications: analytical approach, Opt Laser. Technol. 163 (2023) 109444.
[86] P. Mehrotra, B. Chatterjee, S. Sen, EM-wave biosensors: a review of RF, microwave, mm-wave and optical sensing, Sensors 19 (5) (2019) 1013.
[87] S.M. Ebadi, S. Khani, J. Örtegren, Ultra-compact multifunctional surface plasmon device with tailored optical responses, Results Phys. 61 (2024) 107783.
[88] S.M. Ebadi, S. Khani, J. Örtegren, Design of miniaturized wide band-pass plasmonic filters in MIM waveguides with tailored spectral filtering, Opt. Quant. Electron. 56 (5) (2024) 910.
[89] S.M. Saleh, R. Ali, A. Algreiby, B. Alfeneekh, I.A. Ali, A novel organic chromo-fluorogenic optical sensor for detecting chromium ions, Heliyon 10 (17) (2024) e37480.
[90] D. Citterio, L. Jenny, S. Rásonyi, U.E. Spichiger, Dyes for use in integrated optical sensors, Sensor. Actuator. B Chem. 39 (1–3) (1997) 202–206.
[91] I. Matías Maestro, J. Ascorbe Muruzabal, N.D. Acha Morrás, D. López Torres, P. Zubiate Orzanco, P. Sánchez Zábal, I. Del Villar, Optical sensors based on lossy-mode resonances, Sens. Actuators, B 240 (2017) 174–185, https://doi.org/10.1016/j.snb.2016.08.126.
[92] Y. Chen, M. Ma, F. Tian, Z. Zeng, Z. Xiu, S. Liu, Z. Liu, Temperature and salinity sensing characteristics of embedded core optical fiber based on surface plasmon resonance, Heliyon 9 (11) (2023) e21049.
[93] Y. Zhao, X.G. Li, X. Zhou, Y.N. Zhang, Review on the graphene based optical fiber chemical and biological sensors, Sensor. Actuator. B Chem. 231 (2016) 324–340.
[94] A. Farmani, A. Mir, Graphene sensor based on surface plasmon resonance for optical scanning, IEEE Photon. Technol. Lett. 31 (8) (2019) 643–646.
[95] A.M.R. Zangeneh, A. Farmani, M.H. Mozaffari, A. Mir, Enhanced sensing of terahertz surface plasmon polaritons in graphene/J-aggregate coupler using FDTD method, Diam. Relat. Mater. 125 (2022) 109005.
[96] C. Fenzl, T. Hirsch, O.S. Wolfbeis, Photonic crystals for chemical sensing and biosensing, Angew. Chem. Int. Ed. 53 (13) (2014) 3318–3335.
[97] A.M. Pinto, M. Lopez-Amo, Photonic crystal fibers for sensing applications, J. Sens. 2012 (2012).
[98] C. Lee, B. Lawrie, R. Pooser, K.G. Lee, C. Rockstuhl, M. Tame, Quantum plasmonic sensors, Chem. Rev. 121 (8) (2021) 4743–4804.
[99] H. Im, H. Shao, Y.I. Park, V.M. Peterson, C.M. Castro, R. Weissleder, H. Lee, Label-free detection and molecular profiling of exosomes with a nano-plasmonic sensor, Nat. Biotechnol. 32 (5) (2014) 490–495.
[100] T. Wu, Y. Liu, Z. Yu, Y. Peng, C. Shu, H. Ye, The sensing characteristics of plasmonic waveguide with a ring resonator, Opt Express 22 (7) (2014) 7669–7677.
[101] X. Ren, K. Ren, Y. Cai, Tunable compact nanosensor based on Fano resonance in a plasmonic waveguide system, Appl. Opt. 56 (31) (2017) H1–H9.

[102] Y. Huang, C. Min, S. Tao, G. Veronis, Design of compact Mach–Zehnder interferometer-based slow-light-enhanced plasmonic waveguide sensors, J. Lightwave Technol. 34 (11) (2016) 2796–2803.
[103] S. Pang, Y. Huo, Y. Xie, L. Hao, Tunable electromagnetically induced transparency-like in plasmonic stub waveguide with cross resonator, Plasmonics 12 (2017) 1161–1168.
[104] Y. Xie, Y. Huang, H. Che, W. Zhao, W. Xu, X. Li, J. Li, Theoretical investigation of a plasmonic sensor based on a metal–insulator–metal waveguide with a side-coupled nanodisk resonator, J. Nanophotonics 9 (1) (2015), 093099-093099.
[105] A.O. Zaki, K. Kirah, M.A. Swillam, Integrated optical sensor using hybrid plasmonics for lab on chip applications, J. Opt. 18 (8) (2016) 085803.
[106] Z. Chen, L. Yu, L. Wang, G. Duan, Y. Zhao, J. Xiao, A refractive index nanosensor based on Fano resonance in the plasmonic waveguide system, IEEE Photon. Technol. Lett. 27 (16) (2015) 1695–1698.
[107] N. Jankovic, N. Cselyuszka, Multiple Fano-like MIM plasmonic structure based on triangular resonator for refractive index sensing, Sensors 18 (1) (2018) 287.
[108] N. Cennamo, M. Pesavento, F. Arcadio, B. Morrone, M. Seggio, L. Zeni, Plasmonic sensor combined with a microcuvette device for monitoring molecule binding processes at ultra-low concentrations, Sensor. Actuator. B Chem. (2024) 136050.
[109] J. Hu, X. Wang, H. Lei, M. Luo, Y. Zhang, Plasmonic photothermal driven MXene-based gas sensor for highly sensitive NO2 detection at room temperature, Sensor. Actuator. B Chem. 407 (2024) 135422.
[110] D. Citterio, S. Rásonyi, U.E. Spichiger, Development of new dyes for use in integrated optical sensors, Fresen. J. Anal. Chem. 354 (1996) 836–840.
[111] A. Agarwal, K. Venkatakrishna, B. Tan, Cellular DNA based cancer diagnosis using self-internalized plasmonic sensors, Sensor. Actuator. B Chem. 321 (2020) 128496.
[112] N. Korani, M. Danaie, A plasmonic terahertz perfect absorber based on L-shaped graphene patches and gold rods, Appl. Phys. A 129 (11) (2023) 806.
[113] H. Chen, L. Zhang, Y. Hu, C. Zhou, W. Lan, H. Fu, Y. She, Nanomaterials as optical sensors for application in rapid detection of food contaminants, quality and authenticity, Sensor. Actuator. B Chem. 329 (2021) 129135.
[114] T.H. Kauffmann, M.D. Fontana, Optical sensor of salt concentration: uncertainty evaluation, Sensor. Actuator. B Chem. 161 (1) (2012) 21–27.
[115] N. Khansili, G. Rattu, P.M. Krishna, Label-free optical biosensors for food and biological sensor applications, Sensor. Actuator. B Chem. 265 (2018) 35–49.
[116] X. Yang, E. Hua, H. Su, J. Guo, S. Yan, A nanostructure with defect based on Fano resonance for application on refractive-index and temperature sensing, Sensors 20 (15) (2020) 4125.
[117] J. Guo, X. Yang, Y. Wang, M. Wang, E. Hua, S. Yan, Refractive index nanosensor with simple structure based on Fano resonance, IEEE Photon. J. 12 (4) (2020) 1–10.
[118] D.M. Pozar, Microwave Engineering, fourth ed., John Wiley & Sons, 2011.
[119] M. Soljačić, S.G. Johnson, S. Fan, M. Ibanescu, E. Ippen, J.D. Joannopoulos, Photonic-crystal slow-light enhancement of nonlinear phase sensitivity, JOSA B 19 (9) (2002) 2052–2059.
[120] S. Khani, M. Danaie, P. Rezaei, Realization of a plasmonic optical switch using improved nano-disk resonators with Kerr-type nonlinearity: a theoretical and numerical study on challenges and solutions, Opt Commun. 477 (2020) 126359.
[121] N. Amoosoltani, A. Zarifkar, A. Farmani, Particle swarm optimization and finite-difference time-domain (PSO/FDTD) algorithms for a surface plasmon resonance-based gas sensor, J. Comput. Electron. 18 (4) (2019) 1354–1364.
[122] A. Dolatabady, N. Granpayeh, V.F. Nezhad, A nanoscale refractive index sensor in two dimensional plasmonic waveguide with nanodisk resonator, Opt Commun. 300 (2013) 265–268.
[123] Y.Y. Xie, Y.X. Huang, W.L. Zhao, W.H. Xu, C. He, A novel plasmonic sensor based on metal–insulator–metal waveguide with side-coupled hexagonal cavity, IEEE Photon. J. 7 (2) (2015) 1–12.
[124] Z. Chen, X. Cao, X. Song, L. Wang, L. Yu, Side-coupled cavity-induced Fano resonance and its application in nanosensor, Plasmonics 11 (1) (2016) 307–313.
[125] R. Al Mahmud, M.O. Faruque, R.H. Sagor, A highly sensitive plasmonic refractive index sensor based on triangular resonator, Opt Commun. 483 (2021) 126634.
[126] S. Khani, M. Hayati, An ultra-high sensitive plasmonic refractive index sensor using an elliptical resonator and MIM waveguide, Superlattice. Microst. 156 (2021) 106970.
[127] L. Chen, Y. Liu, Z. Yu, D. Wu, R. Ma, Y. Zhang, H. Ye, Numerical analysis of a near-infrared plasmonic refractive index sensor with high figure of merit based on a fillet cavity, Opt Express 24 (9) (2016) 9975–9983.
[128] Y. Deng, G. Cao, H. Yang, G. Li, X. Chen, W. Lu, Tunable and high-sensitivity sensing based on Fano resonance with coupled plasmonic cavities, Sci. Rep. 7 (1) (2017) 1–8.
[129] S.B. Yan, L. Luo, C.Y. Xue, Z.D. Zhang, A refractive index sensor based on a metal-insulator-metal waveguide-coupled ring resonator, Sensors 15 (11) (2015) 29183–29191.
[130] M.R. Rakhshani, Fano resonances based on plasmonic square resonator with high figure of merits and its application in glucose concentrations sensing, Opt. Quant. Electron. 51 (9) (2019) 1–16.
[131] M.R. Rakhshani, M.A. Mansouri-Birjandi, High-sensitivity plasmonic sensor based on metal–insulator–metal waveguide and hexagonal-ring cavity, IEEE Sensor. J. 16 (9) (2016) 3041–3046.
[132] S. Khani, M. Hayati, Optical sensing in single-mode filters base on surface plasmon H-shaped cavities, Opt Commun. 505 (2022) 127534.
[133] Z. Guo, K. Wen, Q. Hu, W. Lai, J. Lin, Y. Fang, Plasmonic multichannel refractive index sensor based on subwavelength tangent-ring metal–insulator–metal waveguide, Sensors 18 (5) (2018) 1348.
[134] Y.F. Chou Chau, C.T. Chou Chao, H.J. Huang, S.H. Chen, T.S. Kao, H.P. Chiang, A multichannel color filter with the functions of optical sensor and switch, Sci. Rep. 11 (1) (2021) 1–14.
[135] R.H. Sagor, M.F. Hassan, S. Sharmin, T.Z. Adry, M.A.R. Emon, Numerical investigation of an optimized plasmonic on-chip refractive index sensor for temperature and blood group detection, Results Phys. 19 (2020) 103611.
[136] S. Khani, M. Afsahi, Optical refractive index sensors based on plasmon-induced transparency phenomenon in a plasmonic waveguide coupled to stub and nano-disk resonators, Plasmonics 18 (2023) 255–270.
[137] Y. Shahamat, A. Ghaffarinejad, M. Vahedi, Plasmon induced transparency and refractive index sensing in two nanocavities and double nanodisk resonators, Optik 202 (2020) 163618.
[138] C.T.C. Chao, Y.F.C. Chau, A.H. Mahadi, M.R.R. Kooh, N.T.R.N. Kumara, H.P. Chiang, Plasmonic refractive index sensor based on the combination of rectangular and circular resonators including baffles, Chin. J. Phys. 71 (2021) 286–299.
[139] Y.P. Qi, L.Y. Wang, Y. Zhang, T. Zhang, B.H. Zhang, X.Y. Deng, X.X. Wang, Multiple Fano resonances in metal–insulator–metal waveguide with umbrella resonator coupled with metal baffle for refractive index sensing, Chin. Phys. B 29 (6) (2020) 067303.
[140] M.R. Rakhshani, A. Tavousi, M.A. Mansouri-Birjandi, Design of a plasmonic sensor based on a square array of nanorods and two slot cavities with a high figure of merit for glucose concentration monitoring, Appl. Opt. 57 (27) (2018) 7798–7804.
[141] M.R. Rakhshani, M.A. Mansouri-Birjandi, High sensitivity plasmonic refractive index sensing and its application for human blood group identification, Sensor. Actuator. B Chem. 249 (2017) 168–176.
[142] M.R. Rakhshani, M.A. Mansouri-Birjandi, Utilizing the metallic nano-rods in hexagonal configuration to enhance sensitivity of the plasmonic racetrack resonator in sensing application, Plasmonics 12 (4) (2017) 999–1006.
[143] N.L. Kazanskiy, M.A. Butt, S.N. Khonina, Nanodots decorated MIM semi-ring resonator cavity for biochemical sensing applications, Photon. Nanostruct: Fundam. Appl. 42 (2020) 100836.
[144] Y.F. Chou Chau, C.T. Chou Chao, H.J. Huang, N.T.R.N. Kumara, C.M. Lim, H.P. Chiang, Ultra-high refractive index sensing structure based on a metal-insulator-metal waveguide-coupled T-shape cavity with metal nanorod defects, Nanomaterials 9 (10) (2019) 1433.
[145] S. Khani, M. Hayati, Optical biosensors using plasmonic and photonic crystal band-gap structures for the detection of basal cell cancer, Sci. Rep. 12 (1) (2022) 1–19.

[146] Z. Chen, L. Dai, C. Jiang, Polarization-independent plasmon-induced transparency for plasmonic sensing, J. Phys. Appl. Phys. 44 (32) (2011) 325106.
[147] S.G. Shafagh, H. Kaatuzian, M. Danaie, A highly sensitive tunable filter using hybrid 1-D photonic crystal and plasmonic MIM waveguide, Optik 228 (2021) 166174.
[148] L. Hajshahvaladi, H. Kaatuzian, M. Danaie, A high-sensitivity refractive index biosensor based on Si nanorings coupled to plasmonic nanohole arrays for glucose detection in water solution, Opt Commun. 502 (2022) 127421.
[149] B. Moeinimaleki, H. Kaatuzian, A. Mallah Livani, M. Modabberanbeh, Plasmonic refractive index nano sensor based on triplet coupled stub resonators based Fano resonances, IET Optoelectron. 17 (6) (2023) 257–272.
[150] L. Hajshahvaladi, H. Kaatuzian, M. Danaie, Photonic crystal assisted excitation of surface plasmons: a high-resolution refractive index sensor based on a gold spiral in a photonic crystal resonator, Opt. Quant. Electron. 56 (9) (2024) 1417.
[151] M. Danaie, L. Hajshahvaladi, E. Ghaderpanah, A single-mode tunable plasmonic sensor based on an 8-shaped resonator for cancer cell detection, Sci. Rep. 13 (1) (2023) 13976.
[152] M. Setareh, H. Kaatuzian, Sensitivity enhancement of a surface plasmon resonance sensor using Blue Phosphorene/MoS2 hetero-structure and barium titanate, Superlattice. Microst. 153 (2021).
[153] L. Hajshahvaladi, H. Kaatuzian, M. Moghaddasi, M. Danaie, Hybridization of surface plasmons and photonic crystal resonators for high-sensitivity and high-resolution sensing applications, Sci. Rep. 12 (1) (2022) 21292.
[154] S.N. Mustaffa, N.M. Yatim, A.R.A. Rashid, N.M. Yatim, V. Pithaih, N.S. Sha'ari, P.S. Menon, Visible and angular interrogation of Kretschmann-based SPR using hybrid Au–ZnO optical sensor for hyperuricemia detection, Heliyon 9 (12) (2023) e22926.